

WNT7A and PAX6 define corneal epithelium homeostasis and pathogenesis

Hong Ouyang^{1,2}, Yuanchao Xue³, Ying Lin^{1,2}, Xiaohui Zhang^{2†}, Lei Xi^{1,2}, Sherrina Patel², Huimin Cai^{4,5}, Jing Luo², Meixia Zhang⁴, Ming Zhang⁴, Yang Yang^{2†}, Gen Li⁴, Hairi Li³, Wei Jiang⁴, Emily Yeh², Jonathan Lin², Michelle Pei², Jin Zhu², Guiqun Cao⁴, Liangfang Zhang^{2,6}, Benjamin Yu^{7,8}, Shaochen Chen^{2,6}, Xiang-Dong Fu^{2,3,8}, Yizhi Liu¹ & Kang Zhang^{1,2,4,8,9}

The surface of the cornea consists of a unique type of non-keratinized epithelial cells arranged in an orderly fashion, and this is essential for vision by maintaining transparency for light transmission. Cornea epithelial cells (CECs) undergo continuous renewal from limbal stem or progenitor cells (LSCs)^{1,2}, and deficiency in LSCs or corneal epithelium—which turns cornea into a non-transparent, keratinized skin-like epithelium—causes corneal surface disease that leads to blindness in millions of people worldwide³. How LSCs are maintained and differentiated into corneal epithelium in healthy individuals and which key molecular events are defective in patients have been largely unknown. Here we report establishment of an *in vitro* feeder-cell-free LSC expansion and three-dimensional corneal differentiation protocol in which we found that the transcription factors p63 (tumour protein 63) and PAX6 (paired box protein PAX6) act together to specify LSCs, and WNT7A controls corneal epithelium differentiation through PAX6. Loss of WNT7A or PAX6 induces LSCs into skin-like epithelium, a critical defect tightly linked to common human corneal diseases. Notably, transduction of PAX6 in skin epithelial stem cells is sufficient to convert them to LSC-like cells, and upon transplantation onto eyes in a rabbit corneal injury model, these reprogrammed cells are able to replenish CECs and repair damaged corneal surface. These findings suggest a central role of the WNT7A–PAX6 axis in corneal epithelial cell fate determination, and point to a new strategy for treating corneal surface diseases.

Corneal and skin epithelium share many similarities, including a typical morphology of stratified epithelium and maintenance of their stem cells by p63 in the keratin 5/keratin 14⁺ (K5/K14)-expressing basal cell layer in limbus and epidermis^{4–8} (Fig. 1a, b and Extended Data Fig. 1a, b). However, there are marked differences between them. Skin epithelial stem cells (SESCs) move upwards from a deep to suprabasal layers vertically during differentiation^{9,10}, where K5 and K14 are replaced by skin-specific K1 and K10 (ref. 11 and Extended Data Fig. 1c, d). In contrast, LSCs (defined by K19 at the limbus¹², see Fig. 1a and Extended Data Fig. 1e) migrate centripetally for several millimetres to the central cornea during which it undergoes differentiation and K5/K14 are replaced by corneal-specific K3 and K12 (refs 13, 14, Fig. 1c and Extended Data Fig. 1f).

A clear, transparent cornea maintained by CECs is essential for vision. Pathological conversion of CECs into skin-like epithelial cells, as indicated by morphological changes and switches in keratin expression (for example, replacement of cornea-specific K3 and K12 by skin-specific K1 and K10 along with K5⁺ cells at the basal layer; see Fig. 1d), leads to the loss of transparency in the cornea and causes millions of people around the world to suffer from partial or complete blindness³, but the underlying mechanism has remained largely unknown.

To elucidate potential disease mechanisms, we successfully developed a feeder-free cell culture protocol to expand LSCs from human donors, enabling us to generate a homogeneous cell population to delineate key factors involved in controlling LSC cell fate determination and CEC differentiation. Proliferating LSCs were characterized by positive p63 and K19 with a high percentage of mitotic marker Ki67 (Fig. 2a and Extended Data Fig. 1g). We next established a three-dimensional LSC differentiation protocol to establish a three-dimensional CEC sphere structure from a single LSC within 14 to 18 days, as evidenced by strong expression of the CEC-specific markers K3 and K12 (Fig. 2b). The three-dimensional differentiation sphere was further characterized by key differences in gene expression between LSCs and CECs; the latter showed increased expression of K3 (31.2-fold higher) and K12 (24.7-fold higher)

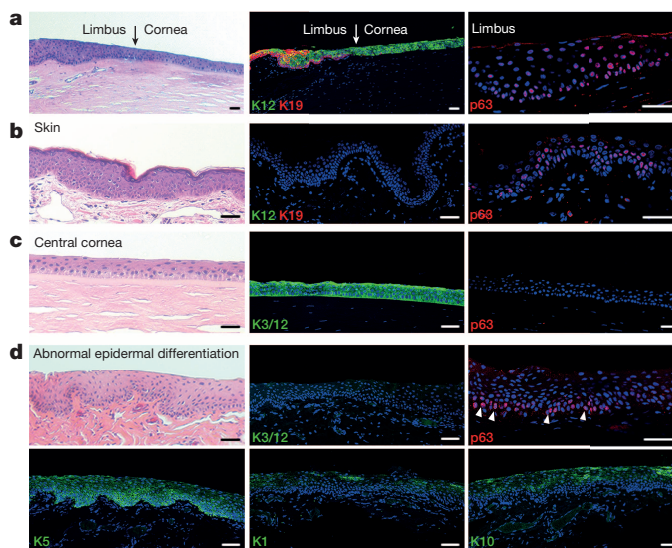


Figure 1 | Normal and pathological changes of corneal epithelium, and its comparison to skin. **a**, Normal cornea–limbus junction (arrows). Limbus identified by K19 and p63 (also see Extended Data Fig. 1e), and cornea by K12. **b**, Normal skin epidermis identified by p63 and K5/K14 (see Extended Data Fig. 1a, b) in the basal layer and absence of K3 and K12 (K3/12). **c**, Normal central cornea labelled by K3/12 and absence of p63 and K1 and K10 (see also Extended Data Fig. 1c, d, f). **d**, Cornea with abnormal epidermal differentiation showing absence of K3/12 (top middle panel) and presence of skin epithelium makers p63 (top right panel) and K5, K1 and K10 (bottom panels). Haematoxylin and eosin (H&E) staining was used for the left panels, with the exception of the bottom left panel. Scale bars, 100 μ m.

¹State Key Laboratory of Ophthalmology, Zhongshan Ophthalmic Center, Sun Yat-sen University, Guangzhou 510060, China. ²Department of Ophthalmology, and Biomaterial and Tissue Engineering Center of Institute of Engineering in Medicine, University of California San Diego, La Jolla, California 92093, USA. ³Department of Cellular and Molecular Medicine, University of California San Diego, La Jolla, California 92093, USA. ⁴Molecular Medicine Research Center, State Key Laboratory of Biotherapy, West China Hospital, Sichuan University, Sichuan 610041, China. ⁵Guangzhou KangRui Biological Pharmaceutical Technology Company Ltd., Guangzhou 510005, China. ⁶Department of Nanoengineering, University of California San Diego, La Jolla, California 92093, USA. ⁷Department of Medicine, University of California San Diego, La Jolla, California 92093, USA. ⁸Institute for Genomic Medicine, University of California San Diego, La Jolla, California 92093, USA. ⁹Veterans Administration Healthcare System, San Diego, California 92093, USA. [†]Present addresses: Beijing Institute of Ophthalmology, Beijing Tongren Eye Center, Beijing 100730, China (X.Z.); Department of Ophthalmology, Shengjing Hospital of China Medical University, Shenyang 110004, China (Y.Y.).

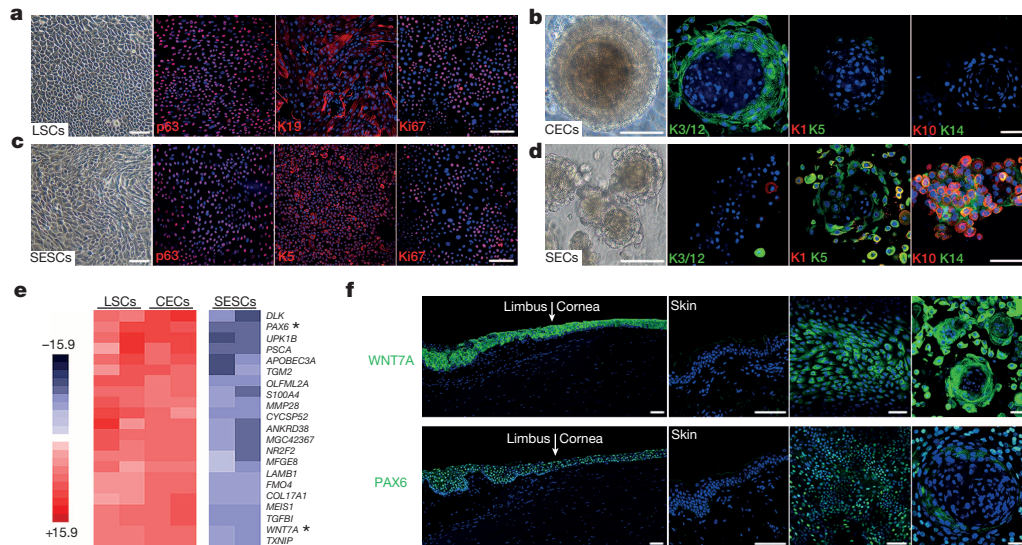


Figure 2 | Exclusive expression of WNT7A and PAX6 at limbus and cornea. **a–d**, Immunofluorescence staining of cultured LSCs and SECs, and three-dimensional differentiated CECs and SECs. Left panels, phase contrast photographs; staining of p63, K19 and Ki67 in LSCs (**a**), p63, K5 and Ki67 in SECs (**c**), K3/12, K1, K5, K10 and K14 in CECs (**b**) and SECs (**d**) in three-dimensional culture spheres. **e**, Heatmap depicting differential gene expression

comparing among LSCs, CECs and SECs. Asterisks indicate WNT7A and PAX6. **f**, Immunofluorescence staining of WNT7A and PAX6 at limbus, cornea and skin (left and middle left panels). Expression of WNT7A and PAX6 in cultured LSCs (middle right panels) and three-dimensional CEC spheres (right panels). Scale bars, 100 μ m.

and concomitant decreased expression of *K19* (6.2-fold lower, all $P < 0.01$; see Extended Data Fig. 1h). We took a similar strategy to expand SECs and observed strong expression of typical SEC markers p63 and K5 in cultured SECs (Fig. 2c). As expected, we detected increased expression of epidermal differentiation markers *K1* (16.6-fold higher) and *K10* (225.8-fold higher) in three-dimensional differentiated skin epithelial cells (SECs) compared to SECs (Fig. 2d, Extended Data Fig. 1i, j).

To identify additional genes uniquely expressed in LSCs, CECs and SECs, we performed genome-wide gene expression analysis (Fig. 2e and Extended Data Fig. 2a, b). Among genes that were differentially expressed, we focused on signalling molecules and transcription factors because of their central roles in cell fate determination and differentiation. We identified that *WNT7A* and *PAX6* were highly expressed in LSCs and CECs when compared to SECs (*PAX6*, 8.8-fold higher in LSCs and 12.3-fold higher in CECs, $P < 0.001$; *WNT7A*, 4.5-fold higher in LSCs, 6.0-fold higher in CECs, $P < 0.001$) (Fig. 2e and Extended Data Fig. 2c). We observed that *WNT7A* expression precisely mirrored the expression pattern of *PAX6* in *in vitro* LSC and CEC cultures, and in *in vivo* epithelial layers of cornea and limbus from infant to adult, while both of these genes were undetectable in skin epidermis (Fig. 2f and Extended Data Fig. 2d).

To determine the clinical relevance of *WNT7A* and *PAX6* expression in LSCs and CECs, we examined several types of human corneal diseases, corneal epithelium squamous metaplasia, inflammatory keratopathy, trauma and alkaline burn. We observed the localized expression of p63 and K5 at the basal layer (Fig. 3a and Extended Data Fig. 3), and the expression of K10 in the suprabasal layer (Fig. 1d and Extended Data Fig. 3). We also found that *WNT7A* and *PAX6* expression, and K3 and K12 expression were conspicuously absent in areas of metaplasia, while they were positive in surrounding corneal epithelium (Fig. 3a and Extended Data Fig. 3). These results suggest cornea epithelial cells were switched to skin-like epithelial cells in patient tissues with these disease conditions.

Wnt molecules are secreted signalling proteins that have a critical role in controlling cell fate decisions and tissue specification¹⁵. *PAX6* is also a well-known control gene for eye development and disease¹⁶. However, it has remained unclear whether the loss of *PAX6* is the cause or the consequence of abnormal skin epidermal differentiation in ocular surface diseases.

To demonstrate that *WNT7A* and *PAX6* are necessary for LSC and CEC cell fate determination and differentiation, we used lentiviral short hairpin RNAs (shRNAs) to knock them down specifically in LSCs. Although LSCs with knockdown of either *WNT7A* or *PAX6* did not change proliferation and morphological properties (Extended Data Fig. 4a), these treatments significantly diminished the expression of corneal K3

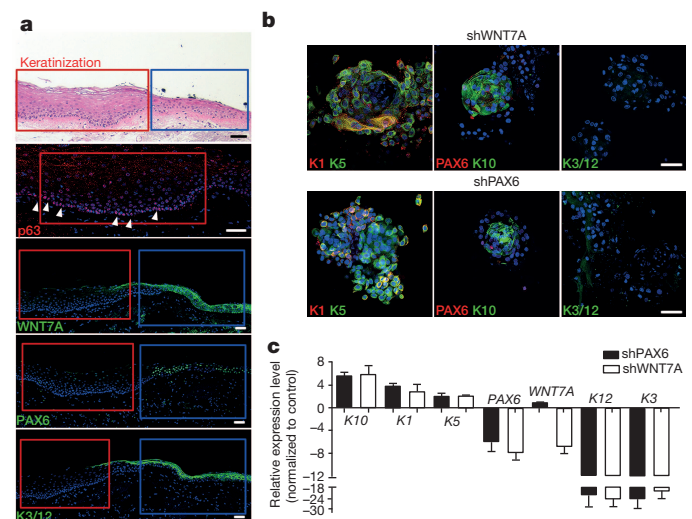


Figure 3 | WNT7A and PAX6 are essential for maintenance of cornea cell fate. **a**, Human corneal epithelium squamous metaplasia. In the top panel, the red box indicates the area of metaplasia and the blue box indicates the area of relatively normal cornea. H&E stain (top panel) shows typical skin epidermal morphology with p63⁺ at basal layer (second panel, arrowheads indicate p63 staining). Loss of *WNT7A* (middle panel) and *PAX6* (fourth panel) was accompanied by absence of corneal K3/12 (bottom panel). Serial sections of the areas marked by red and blue boxes in the top panel are represented in the lower panels. **b**, Immunofluorescence of three-dimensional differentiated cells with *WNT7A* or *PAX6* knockdown; left panels, K1 and K5; middle panels, *PAX6* and K10; right panels, K3/12; **c**, Quantitative PCR analysis of gene expression changes of cornea or skin epithelium markers in three-dimensional differentiated cells with *WNT7A* or *PAX6* knockdown (all $n = 3$, $P < 0.05$). Data are shown as means \pm s.d. Scale bars, 100 μ m.

and K12 under the three-dimensional differentiation conditions (*WNT7A* knockdown: 24.7-fold lower in K3, 22.6-fold lower in K12; *PAX6* knockdown: 20.8-fold lower in K3, 21.4-fold lower in K12; all $P < 0.05$), and concurrently, the expression of skin-specific K1 and K10 became more prominent (*WNT7A* knockdown: 3.9-fold higher in K1 and 5.7-fold higher in K10; *PAX6* knockdown: 3.1-fold higher K1 and 6.1-fold higher in K10; all $P < 0.05$), indicative of more skin-like differentiation (Fig. 3b, c). Moreover, knockdown of *WNT7A* reduced *PAX6* expression in LSCs (1.8-fold lower, $P < 0.001$); this repressive effect was even stronger in differentiated CECs (8.0-fold lower, $P < 0.01$). In contrast, there was no significant difference in *WNT7A* expression when *PAX6* was knocked down in either LSCs or CECs (Fig. 3c and Extended Data Fig. 4b, c). These results suggest that *WNT7A* acts upstream of *PAX6* during CEC differentiation.

To study further the role of the Wnt signalling pathway in corneal fate determination and differentiation, we investigated the functional requirement of Frizzled receptors, which have been shown to interact and transduce *WNT7A* signalling based on co-immunoprecipitation¹⁷. We found that *WNT7A* interacted strongly with Frizzled 5 (*FZD5*) in LSCs (Extended Data Fig. 4d, e), and as predicted, knockdown of *FZD5* in LSCs also led to reduced *PAX6* expression (1.7-fold lower in LSCs and 3.0-fold lower in differentiated CECs ($P < 0.001$) (Extended Data Fig. 4f). Together, these data demonstrated that loss of *WNT7A* or *PAX6* led to a switch of corneal epithelial cells to skin-like epidermal

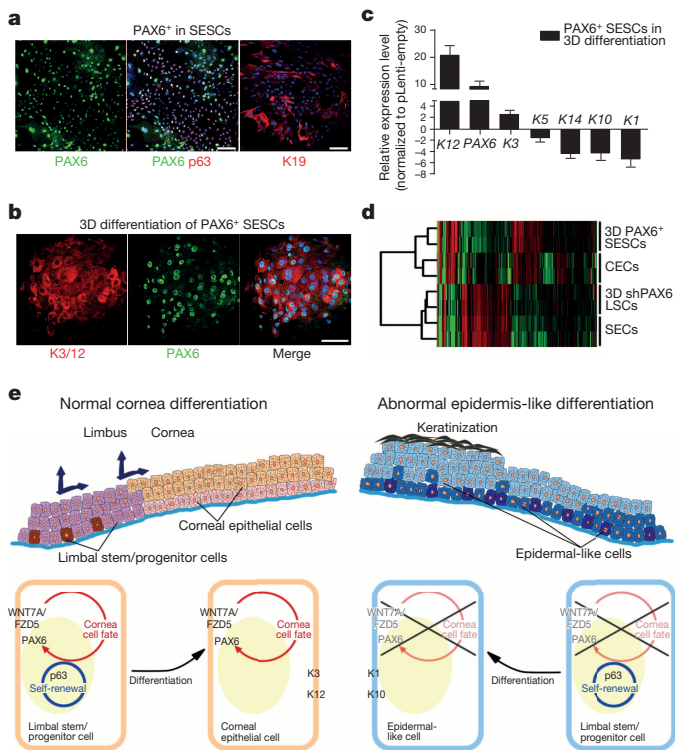


Figure 4 | Conversion of SENCs into corneal epithelial-like cells by *PAX6* transduction. **a**, Double immunofluorescence staining of *PAX6* and p63 in transduced SENCs, K19 was positive in *PAX6*-transduced (*PAX6*⁺) SENCs. **b**, Immunofluorescence staining of K3/12 and *PAX6*⁺ SENCs in three-dimensional (3D) differentiation conditions. **c**, QPCR analysis of gene expression of keratins in *PAX6*⁺ SENCs (all $n = 3$, $P < 0.05$). Data are shown as means ± s.d. **d**, Hierarchical cluster analysis among CECs, differentiated LSCs with *PAX6* knockdown (three-dimensional shPAX6 LSCs), SECs and differentiated SENCs with *PAX6* transduction (three-dimensional *PAX6*⁺ SENCs). **e**, Schematic diagram showing normal LSCs differentiation into CECs (left panel) and proposed mechanism in which loss of *WNT7A*/*PAX6* in LSCs leads to abnormal skin epidermis-like differentiation in corneal surface epithelial cell disease (right panel). Scale bars, 100 μm.

cells and that *WNT7A* and *FZD5* acted as the upstream regulators of *PAX6* expression in corneal differentiation.

Given the central role of *PAX6* in eye development¹⁶, we next tested the possibility that engineered expression of *PAX6* might be able to convert SENCs into LSC-like cells (Extended Data Fig. 5a). Indeed, we found that the expression of either *PAX6a* or *PAX6b* in SENCs was sufficient to convert them into LSC-like cells, as evidenced by the induced K19 expression on the surface, coincident with the expression of both p63 and *PAX6* in the nucleus (Fig. 4a). When placed in three-dimensional culture, *PAX6*-transduced SENCs showed dramatic increase in corneal K3 and K12 expression (9.4-fold higher and 72.7-fold higher, all $P < 0.05$) with concomitant decrease in skin K1 and K10 expression (20.8-fold lower and 20.0-fold lower, all $P < 0.01$) (Fig. 4b, c and Extended Data Fig. 5b, c). To obtain global evidence for successful cell fate conversion, we performed gene expression profiling by RNA sequencing (RNA-seq)¹⁸ on CECs, SECs and LSCs after knocking down *PAX6* and on SENCs transduced with *PAX6* upon three-dimensional differentiation. We generated 3 to 7 million reads from each biological sample that were uniquely

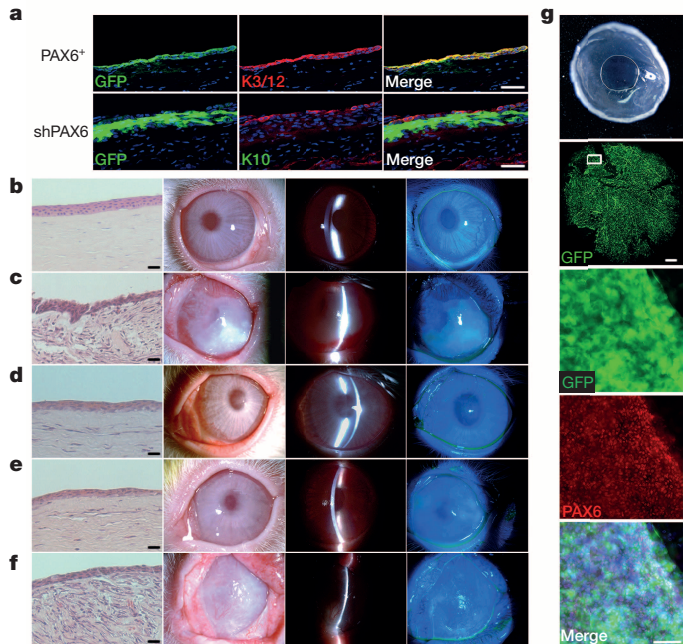


Figure 5 | Cell transplantation and cornea epithelium repair in a rabbit limbal stem cell deficiency model. **a**, Immunofluorescence staining of rabbit corneas 2 months post transplantation. Top panels, cornea transplanted with GFP-labelled *PAX6*⁺ SENCs, showing positive GFP signals and the expression of the corneal epithelium markers K3 and K12 on the corneal surface. Bottom panels, cornea transplanted with GFP-labelled shPAX6 LSCs, showing positive GFP signals and the expression of the skin epidermal epithelium marker K10. Scale bars, 100 μm. **b-f**, Rabbit corneas 2 months post cell transplantation (left panels, H&E stain; middle two panels, white light micrograph and slit-lamp micrograph; right panels, fluorescein dye staining of corneal epithelium surface). Scale bars, 100 μm. **b**, Normal cornea with typical corneal epithelium histology and intact cornea surface without epithelial defects. **c**, Denuded cornea covered with a human amniotic membrane only, showing histology of epithelium metaplasia and opaque cornea with vascularization ($n = 4$). **d, e**, Cornea transplanted with GFP-labelled LSCs (**d**, $n = 3$) and GFP-labelled *PAX6*⁺ SENCs (**e**, $n = 5$), showing corneal epithelium histology, healed and intact cornea surface without epithelial defects. **f**, Cornea transplanted with GFP-labelled, shPAX6-treated LSCs, showing histology of epithelium metaplasia, opaque and vascularized corneal surface with epithelial defects ($n = 4$). **g**, Rabbit cornea 3 months post transplantation with GFP-labelled *PAX6*⁺ SENCs: smooth, transparent cornea (top panel) with positive GFP signals (second panel, scale bar, 1 mm). The framed area in the second panel is enlarged to show the expression of *PAX6* (middle, fourth and bottom panels, scale bar, 100 μm).

mapped to the RefSeq database (Extended Data Fig. 6a). Pairwise comparison demonstrated that the data were very reproducible within the same group of samples (Extended Data Fig. 6b); in contrast, when compared between cells with different fates, the data demonstrate remarkable differences based on the statistical cut-off of false discovery rate (FDR) < 0.001 (Extended Data Fig. 6c). We displayed the entire data sets that recorded the expression of $> 10,000$ genes in various cell types (Fig. 4d), demonstrating that both induced (red) and repressed (green) genes were clearly co-segregated between CECs and PAX6⁺ SESC and between PAX6 shRNA-treated LSCs and SECs. These data therefore provided global evidence for a role of the WNT7A–PAX6 axis in cell fate conversion from SESC to CECs. Together, these data suggest that defects in the WNT7A–PAX6 axis are likely to be responsible for metaplastic conversion of corneal cells to skin epidermal-like cells in corneal diseases in humans (shown in Fig. 4e), although further studies need to be performed to determine the significance of the WNT7 and PAX6 axis in corneal epithelial differentiation.

Finally, we tested the treatment and repair potential of SESC with engineered expression of PAX6 (Extended Data Fig. 7a–c) for corneal epithelial defects in a rabbit LSC deficiency model (Extended Data Fig. 7f), which mimics a common corneal disease condition in humans. We showed that rabbit SESC with PAX6 transduction formed a continuous sheet of epithelial cells with positive staining of corneal-specific K3 and K12 (Fig. 5a) and successfully repaired epithelium defect of the entire corneal surface to restore and maintain normal cornea clarity and transparency for over 3 months (Fig. 5b–g and Extended Data Fig. 8). By following the time course of corneal epithelial surface repair using GFP-labelled PAX6⁺ SESC, we observed that these PAX6-reprogrammed SESC were initially only located at the limbal region and then moved progressively towards the central cornea with corresponding areas of restored cornea clarity (Extended Data Fig. 9a). Importantly, these grafted cells were indeed able to repopulate limbus as evidenced by culture and re-isolation of PAX6⁺ SESC from limbal region (Extended Data Fig. 9b). Notably, these reprogrammed SESC were capable of repairing large corneal epithelium defects after repeated corneal epithelial scraping (Extended Data Fig. 9c). In marked contrast, transplanting rabbit LSCs with PAX6 knockdown (Extended Data Fig. 7a, d, e) onto denuded corneal surface resulted in a K10⁺ skin-like epithelium with opacity and vascularization (Fig. 5f). Together, these data demonstrate that SESC with PAX6 expression are able to trans-differentiate into corneal-like epithelium and repair corneal surface defects.

In summary, this work establishes the feasibility of expanding LSCs under feeder-free conditions and its therapeutic potential, and demonstrates key roles of WNT7A and PAX6 in corneal lineage specification. Importantly, SESC or other cell types converted into a corneal fate by PAX6 expression may serve as a potential source for corneal surface repair and regeneration, particularly in patients with total LSC deficiency. This would overcome a major feasibility problem in using a patient's own reprogrammed LSCs for transplantation, thus pointing to a potential therapeutic strategy for treating many common corneal diseases in humans.

METHODS SUMMARY

LSCs and SESC were isolated from rabbits and human donors in feeder-free media and differentiated in the three-dimensional culture conditions. Histology, immunohistochemistry and immunocytochemistry were carried out on paraffin sections as well as on cultured cells. Gene expression microarray, RNA-seq and quantitative PCR (qPCR) were performed using total RNA isolated from LSCs, SESC and CECs.

Lentiviral RNA interference and engineered-expression study of WNT7A, PAX6 and FZD5 were carried out in LSCs and SESC. Cell transplantation of LSCs and SESC was performed on animal models of corneal injury. Detailed information is provided in the supplement.

Online Content Methods, along with any additional Extended Data display items and Source Data, are available in the online version of the paper; references unique to these sections appear only in the online paper.

Received 14 August 2013; accepted 12 May 2014.

Published online 2 July 2014.

1. Davanger, M. & Evensen, A. Role of the pericorneal papillary structure in renewal of corneal epithelium. *Nature* **229**, 560–561 (1971).
2. Cotsarelis, G., Cheng, S. Z., Dong, G., Sun, T. T. & Lavker, R. M. Existence of slow-cycling limbal epithelial basal cells that can be preferentially stimulated to proliferate: implications on epithelial stem cells. *Cell* **57**, 201–209 (1989).
3. Li, W. *et al.* Down-regulation of Pax6 is associated with abnormal differentiation of corneal epithelial cells in severe ocular surface diseases. *J. Pathol.* **214**, 114–122 (2008).
4. Pellegrini, G. *et al.* p63 identifies keratinocyte stem cells. *Proc. Natl Acad. Sci. USA* **98**, 3156–3161 (2001).
5. Mills, A. A. *et al.* p63 is a p53 homologue required for limb and epidermal morphogenesis. *Nature* **398**, 708–713 (1999).
6. Yang, A. *et al.* p63 is essential for regenerative proliferation in limb, craniofacial and epithelial development. *Nature* **398**, 714–718 (1999).
7. Koster, M. I., Kim, S., Mills, A. A., DeMayo, F. J. & Roop, D. R. p63 is the molecular switch for initiation of an epithelial stratification program. *Genes Dev.* **18**, 126–131 (2004).
8. Rama, P. *et al.* Limbal stem-cell therapy and long-term corneal regeneration. *N. Engl. J. Med.* **363**, 147–155 (2010).
9. Blanpain, C. & Fuchs, E. Epidermal homeostasis: a balancing act of stem cells in the skin. *Nature Rev. Mol. Cell Biol.* **10**, 207–217 (2009).
10. Arwert, E. N., Hoste, E. & Watt, F. M. Epithelial stem cells, wound healing and cancer. *Nature Rev. Cancer* **12**, 170–180 (2012).
11. Kopan, R. & Fuchs, E. A new look into an old problem: keratins as tools to investigate determination, morphogenesis, and differentiation in skin. *Genes Dev.* **3**, 1–15 (1989).
12. Lauweryns, B., van den Oord, J. J. & Missotten, L. The transitional zone between limbus and peripheral cornea. An immunohistochemical study. *Invest. Ophthalmol. Vis. Sci.* **34**, 1991–1999 (1993).
13. Eichner, R., Bonitz, P. & Sun, T. T. Classification of epidermal keratins according to their immunoreactivity, isoelectric point, and mode of expression. *J. Cell Biol.* **98**, 1388–1396 (1984).
14. Schlötzer-Schrehardt, U. & Kruse, F. E. Identification and characterization of limbal stem cells. *Exp. Eye Res.* **81**, 247–264 (2005).
15. Dorsky, R. I., Moon, R. T. & Raible, D. W. Control of neural crest cell fate by the Wnt signalling pathway. *Nature* **396**, 370–373 (1998).
16. Eiraku, M. *et al.* Self-organizing optic-cup morphogenesis in three-dimensional culture. *Nature* **472**, 51–56 (2011).
17. von Maltzahn, J., Bentzinger, C. F. & Rudnicki, M. A. Wnt7a-Fzd7 signalling directly activates the Akt/mTOR anabolic growth pathway in skeletal muscle. *Nature Cell Biol.* **14**, 186–191 (2012).
18. Yu, F.-X. *et al.* Regulation of the Hippo-YAP pathway by G-protein-coupled receptor signalling. *Cell* **150**, 780–791 (2012).

Acknowledgements This study is supported in part by the 973 program (2013CB967504 and 2014CB964900), Project of Fundamental Research Funds (no.2012KF03), State Key laboratory of Ophthalmology, NIH (GM049369), KACST-UCSD Center of Excellence in Nanomedicine, NIH Director's Transformative R01 Program (R01 EY021374) and CIRM.

Author Contributions H.O., X.-D.F., Yiz.L., and K.Z. designed study, interpreted data and wrote the manuscript. H.O., Y.X., Yin.L., X.Z., L.X., H.C., J.L., Mei.Z., Min.Z., Y.Y., H.L., G.L., E.Y., G.C., J.Z. and B.Y. performed the experiments. Y.L., W.J., J.L. and Yiz.L. obtained human samples. S.C., S.P., M.P. and L.Z. contributed to data analysis and interpretation.

Author Information Microarray and RNA sequence information has been submitted to the Gene Expression Omnibus database under accession number GSE32145 and GSE54322. Reprints and permissions information is available at www.nature.com/reprints. The authors declare no competing financial interests. Readers are welcome to comment on the online version of the paper. Correspondence and requests for materials should be addressed to K.Z. (kangzhang@ucsd.edu), X.-D.F. (xdfu@ucsd.edu) or Y.Z.L. (yizlu62@yahoo.com).

METHODS

Human pathology samples. Corneal epithelium squamous metaplasia and all other tissues were obtained as de-identified surgical specimens, fixed in 5% formalin, embedded into paraffin, sectioned and stained for immunofluorescence studies.

Isolation and culture of limbal stem cells and skin epidermal stem cells. Post-mortem human eyeballs were obtained from eye banks and limbus regions were taken and washed in cold PBS with 100 international units (IU) penicillin and $100 \mu\text{g ml}^{-1}$ streptomycin, and cut into small pieces. Cell clusters were obtained by 0.2% collagenase IV digestion at 37°C for 2 h, single cells were obtained by further digestion with 0.25% trypsin-EDTA at 37°C for 15 min. Primary cells were seeded on plastic plates coated with 2% growth factor reduced Matrigel (354230, BD Biosciences). Limbal stem cells from GFP-labelled rats and rabbits were isolated and cultured using the same method as for human LSCs.

Human epidermis was obtained from donor skin biopsy of eye lids, and hair follicles were removed under microscope. Primary human and rabbit epidermal stem cells were isolated from interfollicular epidermis using the same method as described for human limbal stem cells. Culture medium was as follows: DMEM/F12 and DMEM (1:1) with 1/100 penicillin-streptomycin, 10% fetal bovine serum, 10 ng ml^{-1} EGF, $5 \mu\text{g ml}^{-1}$ insulin, $0.4 \mu\text{g ml}^{-1}$ hydrocortisone, 10^{-10} M cholera toxin and 2×10^{-9} M 3,3',5-triiodo-L-thyronine.

All cells used in the current manuscript are from primary cultured cells made in our laboratories, and mycoplasma contamination tests were routinely carried out and were negative.

In vitro three-dimensional differentiation protocol. Three-dimensional differentiation was performed on a 24-well plate or an 8-well chamber. In brief, dissociated single stem cells were embedded in matrigel at 2×10^4 cells per $50 \mu\text{l}$ gel. Three-dimensional structures were formed after 14–18 days culture in a differentiation medium CnT-30 (limbal stem cell differentiation) or CnT-02 (skin epidermal stem cell differentiation) (Cellntec).

Immunofluorescence and laser confocal microscopy. To detect the localization of proteins in cultured cells, cells were fixed with 4% paraformaldehyde for 20 min, then permeabilized with 0.3% Triton X-100-PBS for 5 min twice and blocked in PBS solution containing 5% bovine serum albumin and 0.3% TritonX-100%, followed by an overnight incubation in primary antibodies at 4°C . After three washes in PBS, cells were incubated with secondary antibody. Cell nuclei were counterstained with DAPI (4',6-diamidino-2-phenylindole). For immunofluorescence of paraffin-embedded tissue sections, de-paraffinization was performed, followed by the same immunofluorescence protocol described above.

The following antibodies were used: mouse anti-p63 monoclonal antibody, rabbit anti-K5 monoclonal antibody, mouse anti-K10 monoclonal antibody, mouse anti-K14 monoclonal antibody with biotin labelled, mouse anti-K19 monoclonal antibody, (MA1-21871, RM210650, MS611P0, MS115B0, MS1902P0, Thermo Fisher Scientific), rabbit anti-PAX6 polyclonal antibody (PRB-278P, Covance), mouse anti-K1 monoclonal antibody (sc-376224, Santa Cruz), Rabbit anti-WNT7A polyclonal antibody, mouse anti-K3/K12 monoclonal antibody, rabbit anti-K12 monoclonal antibody (ab100792, ab68260, ab124975, Abcam), mouse anti-Ki67 monoclonal antibody (550609, BD Biosciences), anti-GFP rabbit monoclonal antibody and anti-GFP mouse monoclonal antibody (G10362, A11120, Invitrogen). The secondary antibodies, AlexaFluor-488- or 568-conjugated anti-mouse or rabbit immunoglobulin-G (IgG) (Invitrogen) were used at a dilution of 1:500. Images were obtained using an Olympus FV1000 confocal microscope.

Quantitative PCR. RNA was isolated using an RNeasy kit (Qiagen) and subjected to on-column DNase digestion. Complementary DNA synthesis was performed using a superscript III reverse transcriptase kit according to the manufacturer's instructions (Invitrogen). qPCR was performed by 40-cycle amplification using gene-specific primers (Extended Data Table 1; top) and a Power SYBR Green PCR Master Mix on a 7500 Real Time PCR System (Applied Biosystems). Measurements were performed in triplicates and normalized to endogenous GAPDH levels. Relative fold change in expression was calculated using the $\Delta\Delta\text{CT}$ method (cycle threshold (CT) values < 30). Data are shown as mean \pm s.d. based on three replicates.

Genome-wide gene expression microarray and data analysis. Total RNA was isolated from LSCs, SESC, and differentiated CECs from three-dimensional differentiation assay. Gene expression microarray analysis was performed using an Illumina human genome microarray system, with each sample in biological replicate ($n = 2$ per group; Human HT-12 v4 Expression BeadChip; Illumina, San Diego, California). Raw data were deposited into the GEO database under accession number GSE32145. Expression-level data were generated by the Illumina BeadStudio version 3.4.0 and normalized using quartile normalization. Probes whose expression level exceeded a threshold value of 64 in at least one sample were considered detected. The threshold value was found by inspection from the distribution plots of \log_2 expression levels. Detected probes were sorted according to their q value, which is the smallest false discovery rate (FDR) at which the probe is called significant. FDR was evaluated using significance analysis of microarrays and its implementation

in the official statistical package sam¹⁹. To avoid false positive calls due to spuriously small variances, the percentile of standard deviation values used for the exchangeability factor s_0 in the regularized t -statistic was set to 50. We combined the LESC and CEC samples into one group of four samples, and looked for differentially expressed genes between this group and SESC samples. The top 100 significant genes in this comparison are presented in Extended Data Fig. 2. All genes in this figure are significant at the FDR level of 0.01 or less. A heatmap was created using in-house hierarchical clustering software, and colours qualitatively correspond to fold changes.

RNA-seq and hierarchical cluster analysis. Total RNA was purified by a Picopure RNA isolation kit (Life Technology). RNA-seq was performed as described previously²⁰. In brief, 600 ng of total RNA was first converted to cDNA by superscript III first strand synthesis kit with primer Biotin-B-T. The cDNA was purified by NucleoSpin Gel and PCR Clean-Up Kit column (Clontech) to remove free primers and enzyme. Then terminal transferase (NEB) was applied to block the terminal of a cDNA 3' end. Streptavidin-coated magnetic beads (Life Technology) were further applied to isolate cDNAs. After RNA degradation by sodium hydroxide, second-strand cDNA was synthesized by random priming with primer A-N8. The second strand cDNA was eluted from beads by heat denaturing. The cDNA was then used as template to construct libraries by amplifies with barcode primers and primer PB. The sequencing was done on Hiseq 2000 system.

Hierarchical cluster analysis was performed with cluster and Java TreeView²¹. The raw data were first filtered using default parameters provided by the program Cluster. The filtered data were further adjusted by log transformation, genes and arrays were centred by median, and then both gene and array were hierarchically clustered with euclidean and average linkage. The hierarchical trees and gene matrix were visualized and generated by Java Treeview.

Lentiviral RNA interference and PAX6 transduction. Lentiviral shRNAs targeting PAX6, WNT7A and FZD5 genes were either cloned into pLKO.1 plasmid between Age I and EcoR I or purchased directly from Sigma. shRNAs targeting sequences for gene-specific knockdowns were as follows: PAX6, CGTCCATCTT TGCTTGGGAAA and AGTTTGAGAGAACCATTATC; WNT7A, CGTGCT CAAGACAAGTACAA and GCGTTCACCTACGCCATCAT; FZD5, CGCG AGCCCTTCGTGCCATT and TCCTAAGGTTGGCGTTGTAAT. We used a lentiviral pLKO.1-puro Non-Target shRNA control plasmid encoding a shRNA that did not target any known genes from any species as a negative control in all gene knockdown experiments (Sigma).

Lentiviral shRNA particles were prepared according to a previous described protocol²². In brief, replication-incompetent lentiviral particles were packaged in 293T cells by co-transfection of shRNA constructs with packaging mix (pCMV-dR8.2 and pCMV-VSVG at a 9:1 ratio). Virus was collected two times at 48 h and 72 h post transfection.

For transduction, PAX6a open reading frame (ORF) was PCR amplified from cDNAs purchased from Thermo Scientific (MHS6278-202756612) and inserted into pLenti CMV-GFP Puro vector between BamHI and BsrGI. PAX6b was generated by PCR-mediated point mutation strategy with primers PAX6 InF and PAX6 InR (Extended Data Table 1; top). For GFP labelling, pLenti CMV-GFP Hygro (656-4) purchased from Addgene was used. The lentiviral particles were packaged by co-transfection with packaging plasmids psPax2 and pMD2.G.

For lentiviral infection, cells were infected for 16–20 h with fresh media containing individual virus and polybrene at a final concentration of $8 \mu\text{g ml}^{-1}$. The infected cells were further selected by $2 \mu\text{g ml}^{-1}$ uramycin for 48 h or $200 \mu\text{g ml}^{-1}$ hygromycin for 72 h.

Western blot analysis and co-immunoprecipitation. For western blot analysis, cells were washed once with PBS and then collected in cell lysis buffer (50 mM Tris-HCl, pH 6.8; 2% SDS; 10% Glycerol; 100 mM DTT). Protein concentration was quantified by Nanodrop and Bromophenol blue was added to a final concentration of 0.1%, then 25 μg of total lysate was fractionated on a 4–12% NUPAGE gel (Life Technology). Proteins were transferred to a nitrocellulose membrane at 100 V for 1 h. The membrane was blocked with 5% milk and probed with relevant antibodies and mouse anti- β -actin monoclonal antibody (A5316, Sigma).

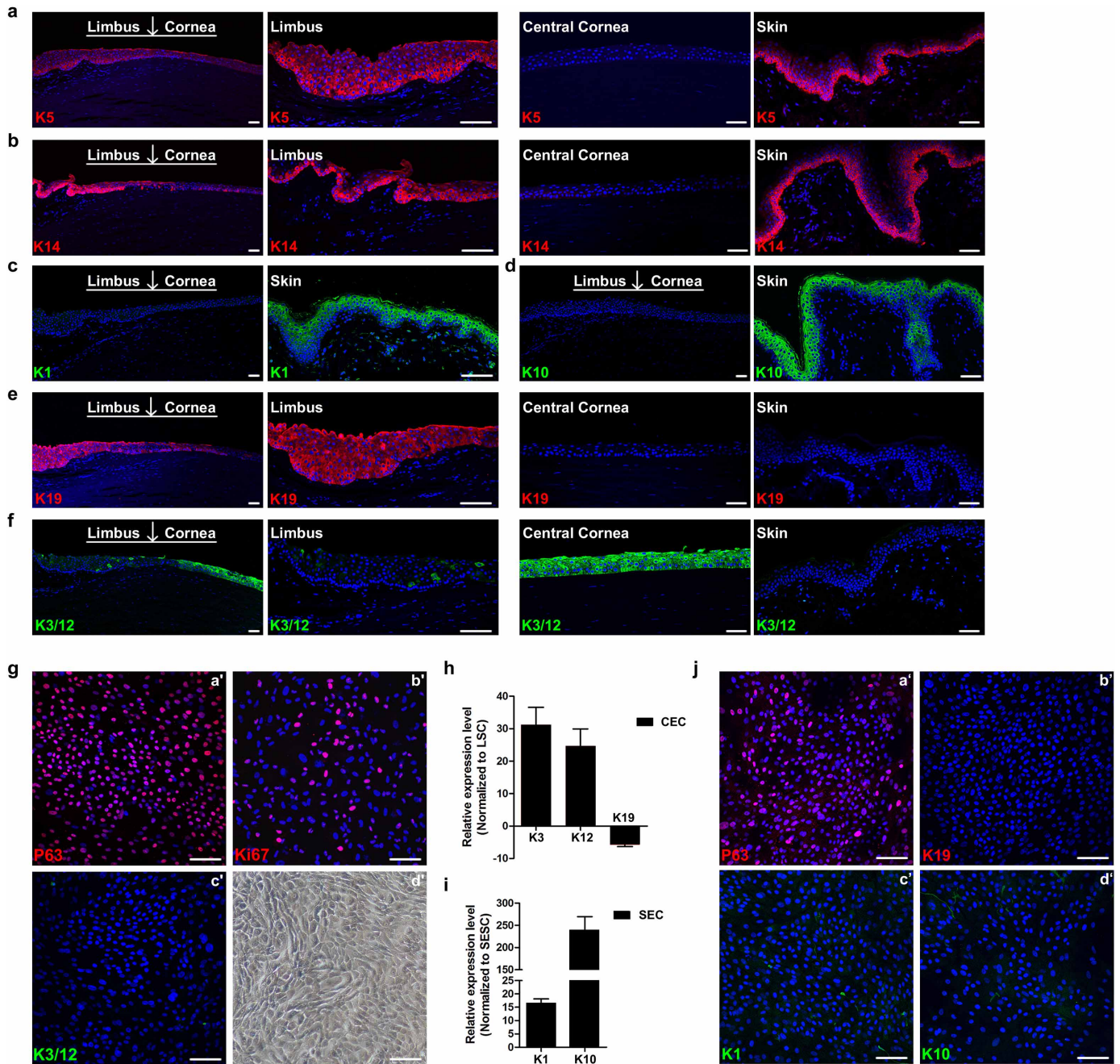
To detect interaction between FZD5 and WNT7A, a 10-cm dish of limbal stem cells at 90% confluence was collected; the cell pellet was resuspended in $700 \mu\text{l}$ of co-immunoprecipitation (Co-IP) buffer (10 mM Tris-HCl, pH 7.4, 100 mM NaCl, 2.5 mM MgCl_2 , 0.5% NP-40, $1 \times$ proteinase inhibitor) and incubated on ice for 20 min, then centrifuged at 13,000 r.p.m. at 4°C for 20 min. The $600 \mu\text{l}$ of supernatant were aliquoted into two pre-chilled Eppendorf tubes, $5 \mu\text{g}$ of rabbit anti-FZD5 monoclonal antibody (#5266, Cell Signaling) or WNT7A antibodies was added to each tube and incubated at 4°C overnight. Protein A/G magnetic beads ($50 \mu\text{l}$, Thermo Fisher) were added to each tube, and incubated at 4°C for 2 h, washed with a Co-IP buffer and eluted in $1 \times$ SDS sample buffer (Life Technology) at 70°C . The input and elutes were fractionated on 4–12% NUPAGE gel and blotted with FZD5 and WNT7A antibodies.

Cell transplantation. All animal studies were performed in full accordance with the Association for Research in Vision and Ophthalmology (ARVO) statement, Use of Animals in Ophthalmic and Vision Research, and approvals were obtained from Institutional Animal Care Committees.

New Zealand white rabbits (2.0 kg to 2.5 kg, male) were used in the study. Rabbits were anaesthetized with intramuscular injection of xylazine hydrochloride (2.5 mg ml^{-1}) and ketamine hydrochloride (37.5 mg ml^{-1}). To create a limbal stem cells deficiency model (Extended Data Fig. 7f), corneal and limbal epithelium was removed by 360-degree conjunctival peritomy and lamellar dissection to remove anterior scleral and corneal stromal tissues, 2 mm posterior from limbus towards the centre of the cornea. This dissection ensured removal of LSC and the entire corneal epithelium. Rabbit GFP-labelled LSCs (5×10^5), PAX6⁺ SESC or shPAX6 LSCs cells were mixed with fibrin (25 mg ml^{-1}) and thrombin (25 U per ml) and seeded onto the exposed stromal bed of a recipient cornea and limbal area; the surface was then covered by a human amniotic membrane (Bio-tissue), which is secured with 10.0 VICRYL sutures (Ethicon) (Extended Data Table; bottom). As a negative control, only amniotic membrane was applied to the denuded cornea. Antibiotics (levofloxacin) and steroids (betamethasone) were applied to both eyes

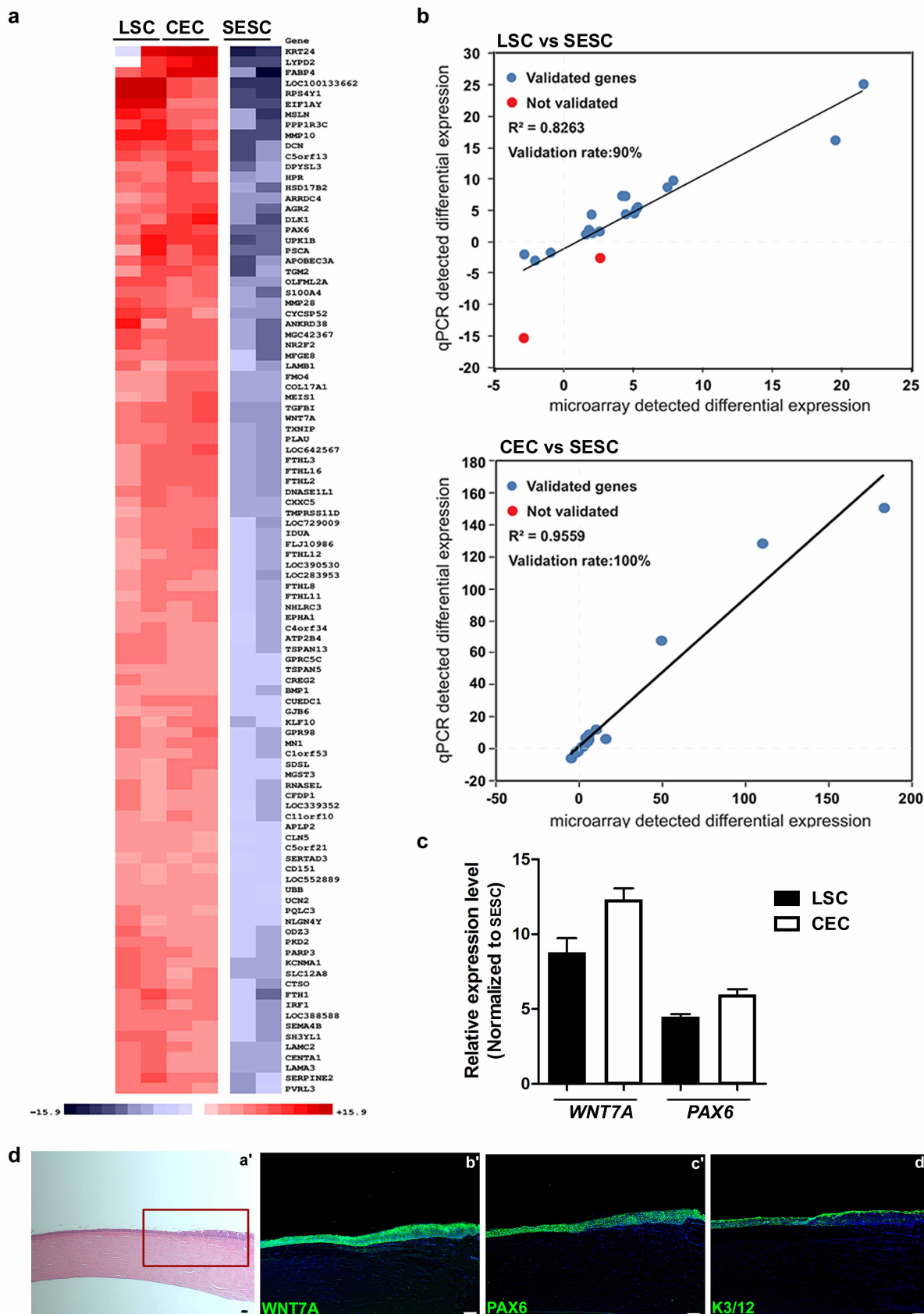
immediately after the cell transplant procedures, and were administered three times a day for 2 weeks. Animals were randomly assigned into each experimental group. The investigator who performed cell transplantation was blind to the identity of cells used. Another investigator carried out assessment of the effect of corneal epithelial repair in rabbits and was again blind to the identity of cells used in the transplantation. For analysis, we exclude only animals that died of post-operative complications such as infection, as they did not reach the end point for assessment of cell transplantation effect; this criterion is pre-established.

19. Tusher, V. G., Tibshirani, R. & Chu, G. Significance analysis of microarrays applied to the ionizing radiation response. *Proc. Natl Acad. Sci. USA* **98**, 5116–5121 (2001).
20. Fox-Walsh, K., Davis-Turak, J., Zhou, Y., Li, H. & Fu, X. D. A multiplex RNA-seq strategy to profile poly(A⁺) RNA: application to analysis of transcription response and 3' end formation. *Genomics* **98**, 266–271 (2011).
21. Eisen, M. B., Spellman, P. T., Brown, P. O. & Botstein, D. Cluster analysis and display of genome-wide expression patterns. *Proc. Natl Acad. Sci. USA* **95**, 14863–14868 (1998).
22. Xue, Y. *et al.* Direct conversion of fibroblasts to neurons by reprogramming PTB-regulated microRNA circuits. *Cell* **152**, 82–95 (2013).



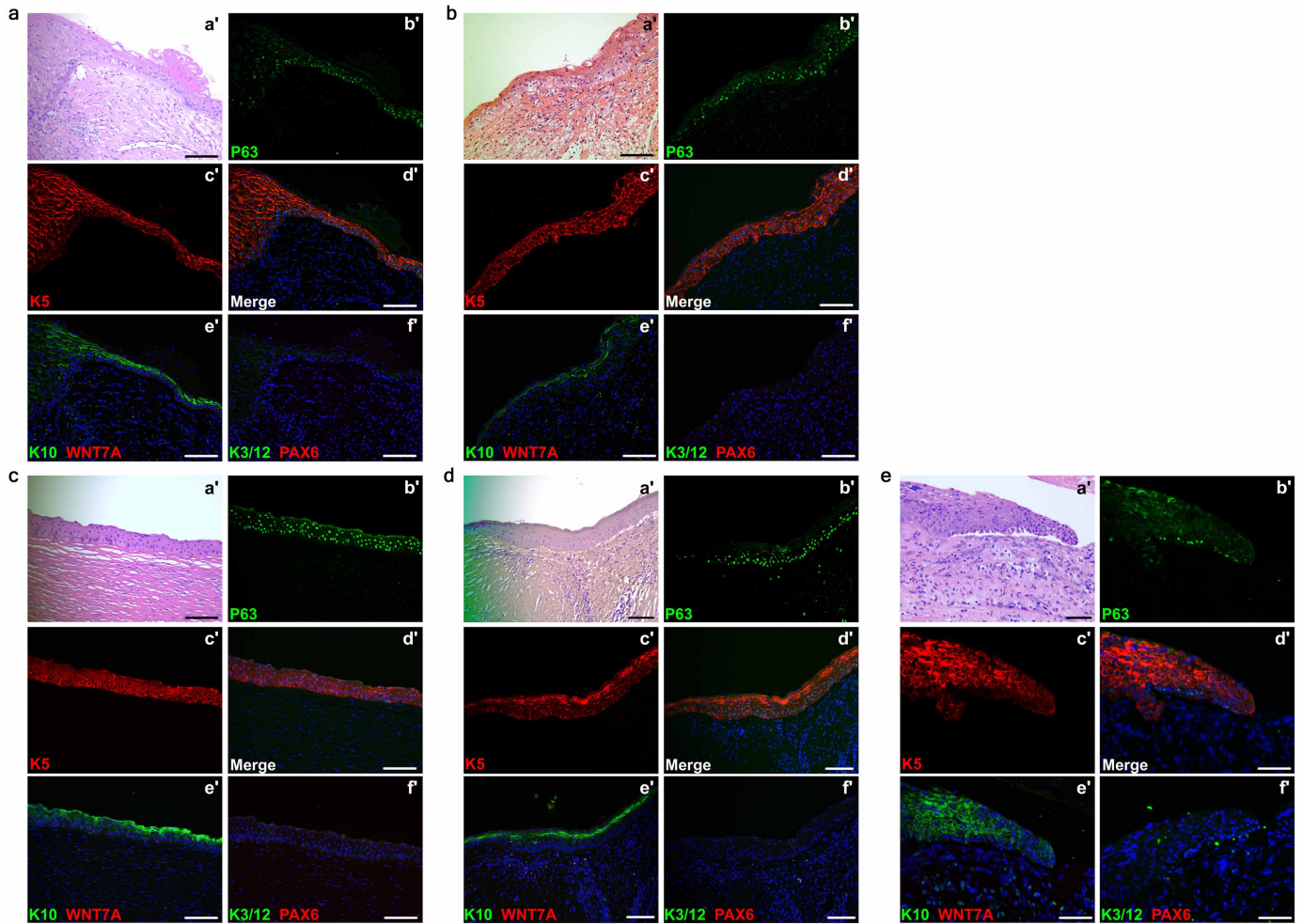
Extended Data Figure 1 | Keratin expression profiles and cell cultures, and three-dimensional differentiation of LSCs and SESC. a–f, Keratin expression profiles in human limbus, cornea and skin epidermis. a, b, Peripheral cornea–limbus junction and skin tissues showing K5⁺ (a) and K14 (b) expression in the basal cell layer of limbus and skin, and their absence in central corneal epithelium. c, d, Skin epidermis showing positive K1 (c) and K10 (d) expression and their absence in cornea and limbus. e, f, Peripheral cornea–limbus junction showing K19⁺ staining in limbus but not in central corneal epithelium and skin (e), and K3/12⁺ staining only in cornea and not in limbus and skin (f). g–j, Cultured LSCs with stem and progenitor cell characteristics, and SESC characteristics at passage 12 and validation of a

three-dimensional differentiation system. g, Immunofluorescence staining of LSCs showing positive stem cell signals of p63 (a') and Ki67 (b') and negative differentiated CEC signals, K3/12 (c'), phase contrast photograph (d'). h, qPCR analysis showing K3/12 upregulation and K19 downregulation in CECs from a three-dimensional differentiation assay compared with LSCs. i, K1 and K10 upregulation in SESC from three-dimensional differentiation assay compared with SESC (c), all $n = 3$, $P < 0.01$. j, Immunofluorescence staining of cultured SESC showing positive p63 (a') and negative signals for limbus stem cell marker, K19 (b') and mature skin epithelium markers K1 and K10 (c', d'). Scale bars, 100 μm . Data shown as means \pm s.d.



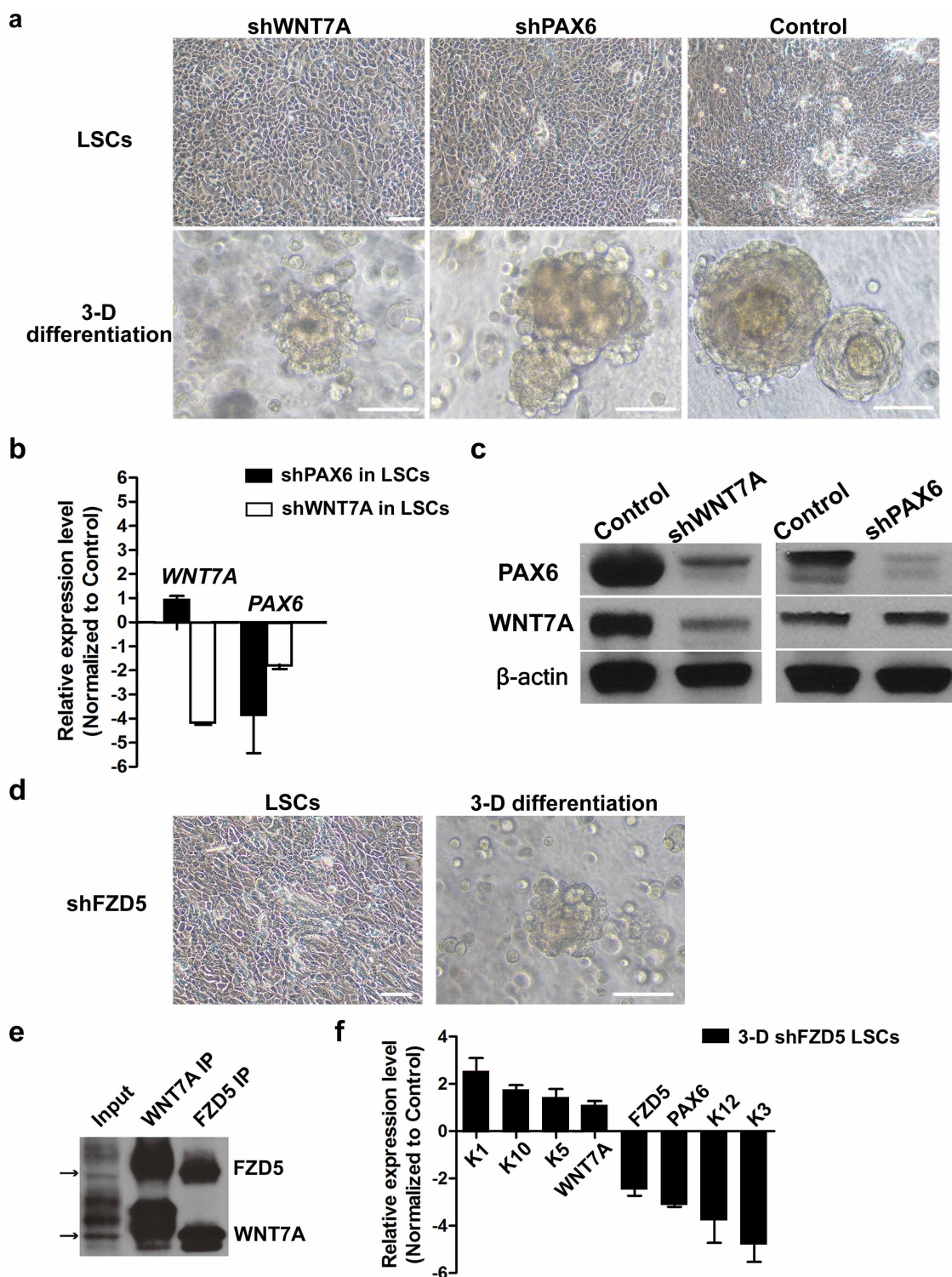
Extended Data Figure 2 | Gene expression profiling and immunohistological analysis. a–c, Genome-wide gene expression microarray of LSCs, CECs and SESC. a, The top 100 significant genes in a comparison of LSCs and CECs to SESC. b, Validation of the microarray data with qPCR analysis showing a strong correlation. c, qPCR analysis of *WNT7A* and *PAX6*

expression in LSCs and CECs compared to SESC, all $n = 3$, $P < 0.05$. d, Expression of *WNT7A* and *PAX6* in cornea and limbus of a one-year old human infant. H&E stain (a'), boxed area was shown in serial sections (b'–d') with immunofluorescence staining of *WNT7A* (b'), *PAX6* (c') and *K3/12* (d'). All scale bars, 100 μm . Data shown as means \pm s.d.



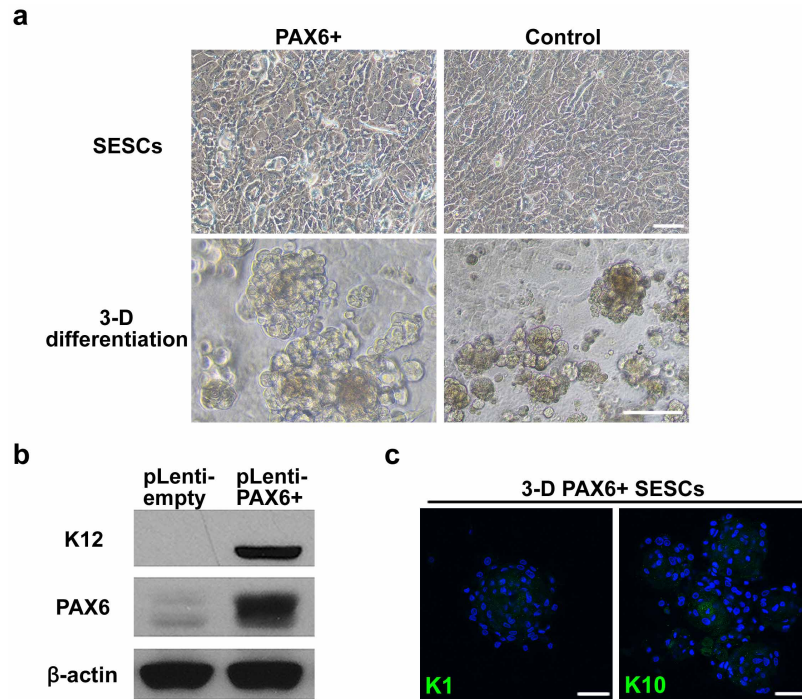
Extended Data Figure 3 | Appearance of skin epidermal markers with loss of corneal markers in human corneal diseases. Appearance of skin epidermal markers p63, K5 and K10 with loss of corneal marker K3/12, PAX6 and WNT7A in cornea of patients with Stevens–Johnson syndrome (a, b), ocular pemphigoid (c), trauma injury (d) and alkaline burn (e). For all images, H&E

staining was carried out on the lesion of corneal epithelial squamous metaplasia (a'). b'–f', the same region of lesion in serial sections showing increased p63 (b', d') and K5 (c', d') and K10 (e') in the suprabasal layer, no WNT7A (e'), K3/12 or PAX6 could be detected in the area (f'). Scale bars, 100 μm .



Extended Data Figure 4 | The effect of *WNT7A* and *FZD5* on *PAX6* expression in LSCs. **a–c**, The effect of *WNT7A* knockdown on *PAX6* expression in LSCs. **a**, Phase contrast photographs showing effects of *WNT7A* and *PAX6* knockdowns (shWNT7A and shPAX6) in LSCs and their three-dimensional differentiation spheres. **b**, qPCR analysis of gene expression changes of *WNT7A* and *PAX6* in LSCs. *WNT7A* knockdown decreased *PAX6* expression ($n = 3$, $P < 0.01$); no significant change in *WNT7A* expression in *PAX6* knockdown. **c**, Validation of knockdown efficiency of *WNT7A* and *PAX6* in LSCs by western blot analysis. **d–f**, *WNT7A* and *FZD5* acted as the

upstream regulators of *PAX6* expression. **d**, Phase contrast photographs showing cell morphology of knockdown of *FZD5* (shFZD5) in LSCs and three-dimensional differentiation spheres. **e**, Co-immunoprecipitation of *WNT7A* and *FZD5* in LSCs. **f**, qPCR analysis of gene expression changes in corneal and skin epithelial markers in three-dimensional differentiated cells of LSCs with *FZD5* knockdown (three-dimensional shFZD5 LSCs). *FZD5* knockdown did not affect *WNT7A* expression; all others, $n = 3$, $P < 0.05$. Scale bars, 100 μm . Data shown as means \pm s.d.



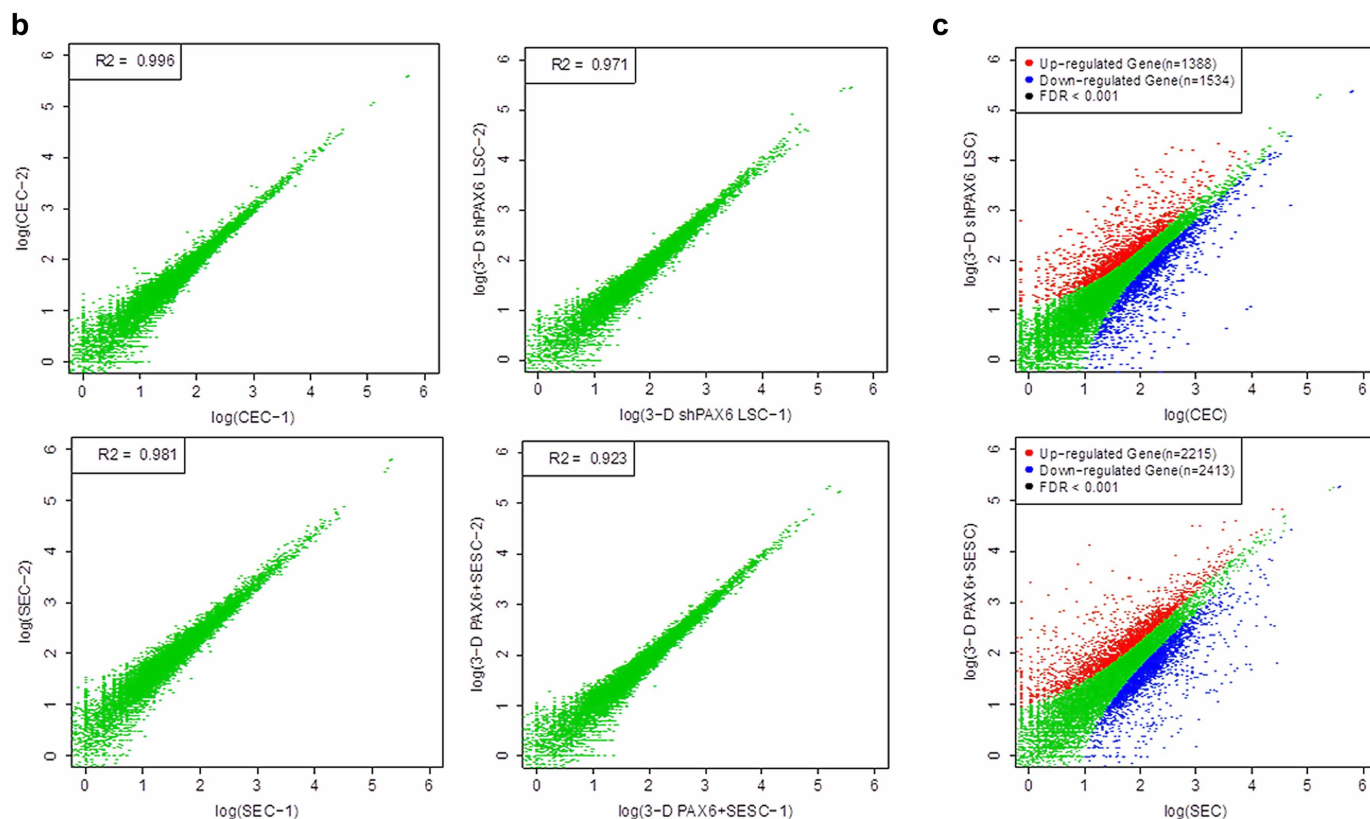
Extended Data Figure 5 | The effect of PAX6 transduction in SESC.

a, Phase contrast photographs of SESC with PAX6 transduction (PAX6⁺) and three-dimensional differentiation spheres. **b**, Validation of K12 and PAX6 expression in three-dimensional differentiation spheres by western blotting

analysis. **c**, Loss of skin-specific keratins, K1 and K10 in three-dimensional differentiation of SESC with PAX6 transduction (three-dimensional PAX6⁺ SESC). Scale bars, 100 μm.

a

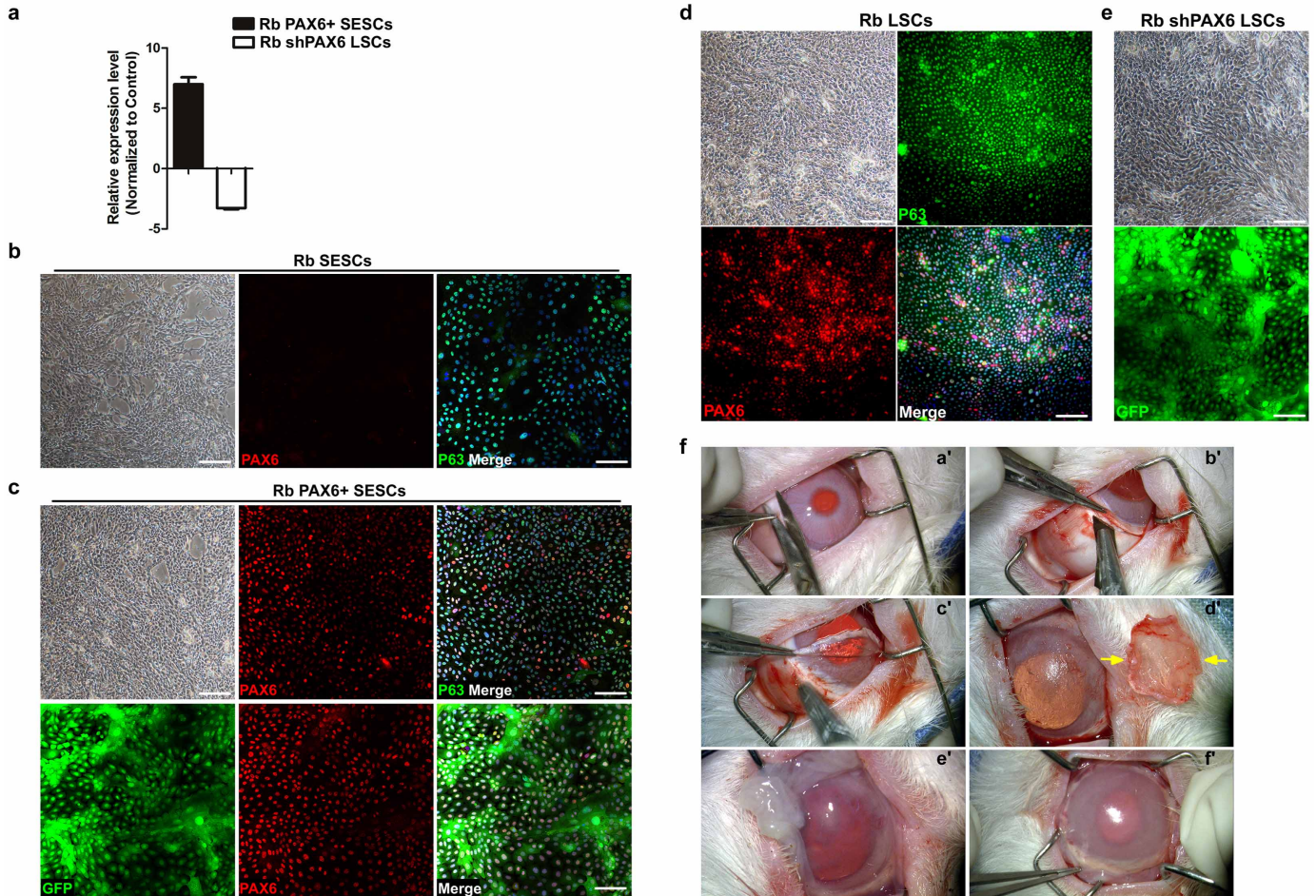
Sample	Raw Reads	Mapping Reads	Mapping Rate
CEC-1	4831619	3221767	0.667
CEC-2	4926847	3089309	0.627
SEC-1	4590757	2776526	0.605
SEC-2	11971991	7073156	0.591
3-D shPAX6 LSC-1	8946779	5345343	0.597
3-D shPAX6 LSC-2	7370502	4462113	0.605
3-D PAX6+SESC-1	6872086	4594613	0.669
3-D PAX6+SESC-2	6347059	4191302	0.660



Extended Data Figure 6 | Quantitative information from RNA-seq data.

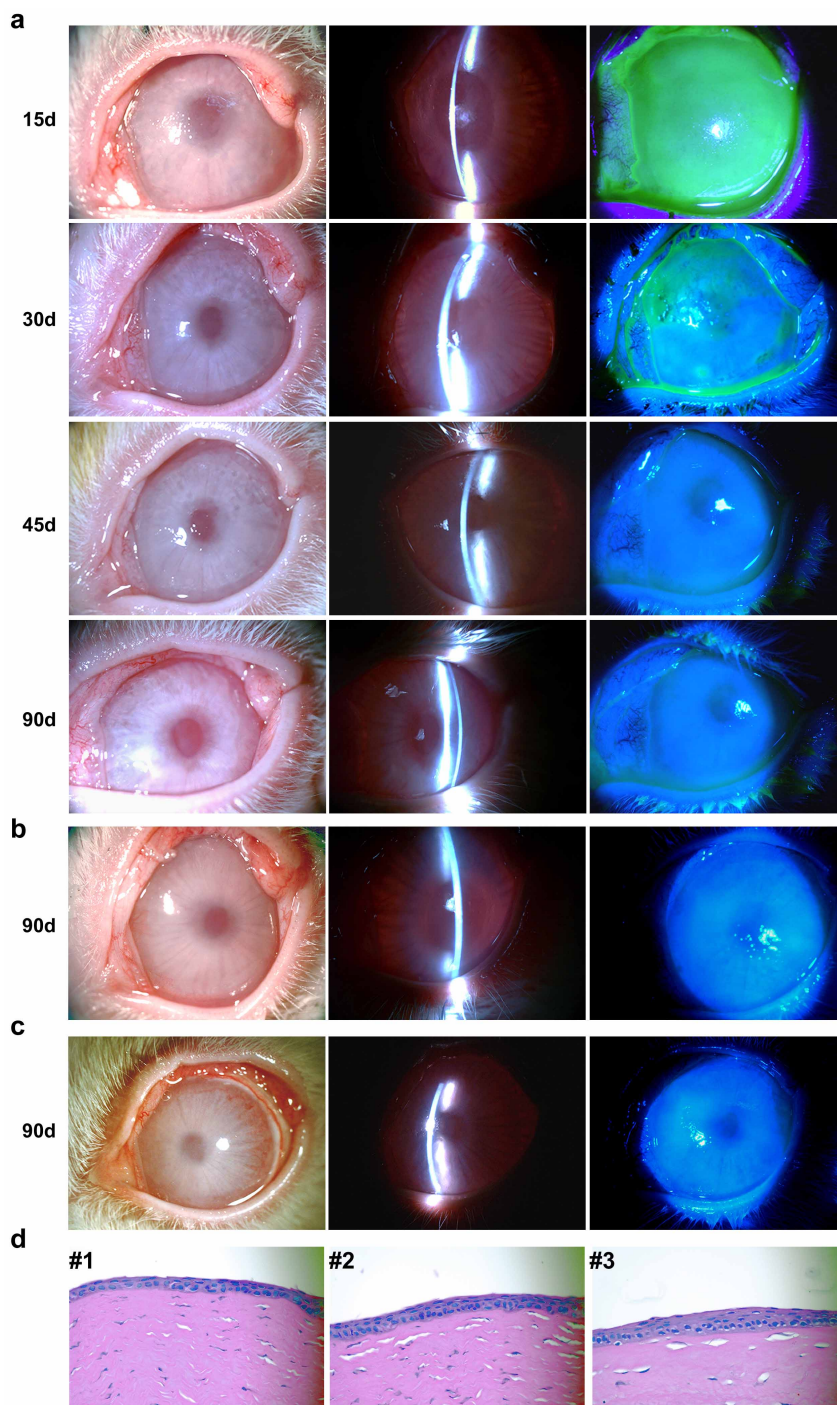
a, Statistical analysis of RNA-seq samples: raw reads, mapping reads and mapping rate of each sample are included. **b**, Pairwise comparisons of duplicated biological samples. **c**, The differences between SECs and three-dimensional PAX6⁺ SESC, CECs and three-dimensional shPAX6 LSCs, all FDR < 0.001. **a**, qPCR analysis of PAX6 expression in rabbit SESC with PAX6 transduction (rabbit (Rb) PAX6⁺ SESC) or LSCs with PAX6 knockdown

(Rb shPAX6 LSCs) (all $n = 3$, $P < 0.05$). We noticed some minor differences in the heatmap. These might result from some experimental variations, or it is possible that, although PAX6 expression is largely responsible for cell fate switch from SESC to CECs at gene expression and functional levels (as demonstrated in this study), this single transcription factor may not be sufficient to create cells that are completely identical to CECs.



Extended Data Figure 7 | Engineered expression of PAX6 and rabbit LSC deficiency model. **a–e**, Quantification and culture of engineered expression of PAX6 in rabbit SESC and PAX6 knockdown LSC. **a**, qPCR analysis of PAX6 expression in rabbit SESC with PAX6 transduction (Rb PAX6⁺ SESC) or LSC with PAX6 knockdown (Rb shPAX6 LSC) (all $n = 3$, $P < 0.05$). **b**, Rabbit SESC with positive staining of p63 and negative staining of PAX6. Left panel, phase contrast photograph. **c**, Top row, double immunofluorescence staining of PAX6 and p63 in rabbit SESC with PAX6 transduction. Top left panel, phase contrast photograph. Bottom row, rabbit PAX6⁺ SESC were further

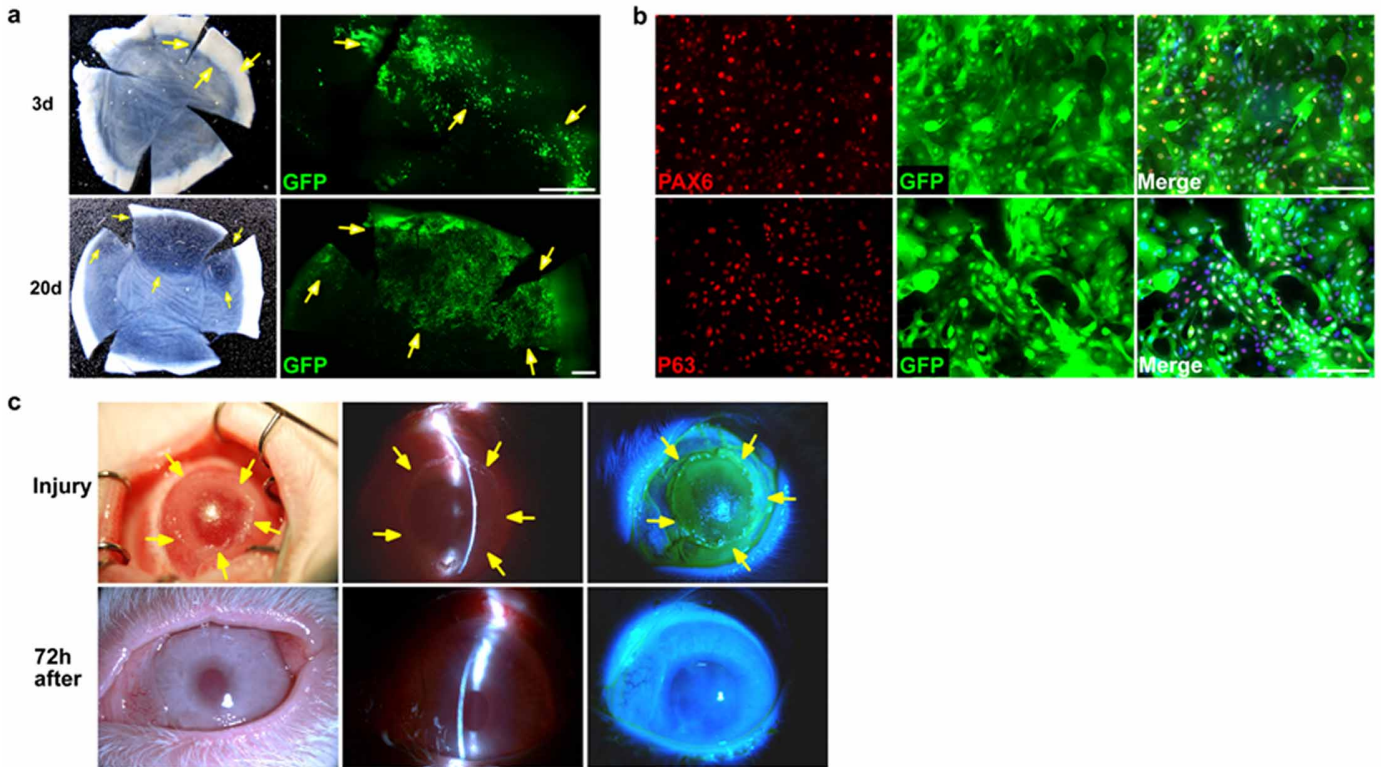
labelled with GFP for transplantation. **d**, Rabbit LSC with positive staining of p63 and PAX6. Top left panel, phase contrast photograph. **e**, Culture of GFP-labelled rabbit LSC with PAX6 knockdown. **f**, conjunctiva peritomy was performed and a circumferential strip of 2mm anterior limbal conjunctiva was removed (**a'**). Lamellar scleral and corneal dissection to completely remove LSC and corneal epithelium along an anterior cornea stroma plane (**b'–d'**). Dissected cap is shown in (**d'**, arrows). The exposed cornea stroma bed was covered by human amniotic membrane (**e'**) and sutures (**f'**). ($n = 3$). Scale bars, 100 μm . Data shown as means \pm s.d.



Extended Data Figure 8 | Cornea epithelium regeneration and repair by transplanted GFP-labelled PAX6⁺ SESC in a rabbit LSC deficiency model.

a, Time course of corneal epithelial defect repair. Fifteen days post transplantation, there was decreased cornea clarity with an entire corneal epithelial defect evidenced by fluorescein stain of cornea surface; 30 days post transplantation there was improved cornea clarity and reduced fluorescein staining of cornea epithelial defect; 45 and 90 days post transplantation there was restoration and maintenance of cornea clarity. **b, c**, Two other examples of regeneration and repair of rabbit corneal epithelial surface 90 days post

transplantation with GFP-labelled PAX6⁺ SESC showing complete repair and re-epithelization of corneal epithelial defects. Left panels, white light micrographs; middle panels, slit-lamp micrographs; right panels, fluorescein staining (note that bright spots on the corneal surface were due to camera light reflection, they were not epithelial defects) of corneal epithelium ($n = 5$). **d**, H&E stain of regeneration and repair of corneal epithelial surface in three separate rabbits 90 days post transplantation with GFP-labelled PAX6⁺ SESC showing intact corneal epithelium histology.



Extended Data Figure 9 | Corneal epithelial regeneration by transplantation in a rabbit LSC deficiency model. **a**, Time course of corneal epithelial regeneration and repair in a rabbit LSC deficiency model post transplantation with GFP-labelled PAX6⁺ SENCs. Top panels, 3 day post transplantation. Left, light micrograph showing a hazy cornea; right, GFP⁺ donor cells at limbal region (arrows). Bottom panels, 20 days post transplantation. Left, light micrograph showing a cornea with partial clarity; right, GFP⁺ donor co-located in transparent areas (arrows). Scale bars, 1 mm. We observed that only the transplanted cells from the limbal region could survive, proliferate and regenerate cornea surface epithelium, suggesting that limbus contained the stem cell niche favourable for stem cell survival and growth. **b**, Culture and re-isolation of reprogrammed donor GFP-labelled

PAX6⁺ SENCs epithelial cells from the limbal region of a rabbit recipient eye 90 days post transplantation with GFP-labelled PAX6⁺ SENCs. Top panel, double immunofluorescence staining of PAX6 and GFP; bottom panel, double immunofluorescence staining of p63 and GFP in PAX6-transduced rabbit SENCs. Scale bars, 100 μ m. **c**, Repair and recovery of a repeat cornea epithelium injury on a cornea transplanted with GFP-labelled PAX6⁺ SENCs. Top panels, we iatrogenically scraped and removed donor-derived corneal epithelial cells and made a large corneal surface epithelium defect (arrows) 3 months post initial transplantation of PAX6⁺ SENCs. Bottom panels, complete repair and recovery were observed within 72 h with healed epithelial defect ($n = 3$). Left panels, light micrographs; middle panels, slit-lamp micrographs; right panels, fluorescein staining.

Extended Data Table 1 | Primer sequences and rabbit transplantation results

Extended Data Table 1a. Primer sequences

Gene (Human)	Forward Primer	Reverse Primer
<i>CASZ1</i>	<i>GTTCTACGGACAGAAGACCACG</i>	<i>TCTTGAAGCCGTCCTTGGCGTA</i>
<i>FGFR3</i>	<i>AGTGGAGCCTGGTCATGGAA</i>	<i>GGATGCTGCCAAACTTGTCTC</i>
<i>FZD5</i>	<i>TGGAACGCTTCCGCTATCTGA</i>	<i>GGTCTCGTAGTGGATGTGGTTG</i>
<i>GAPDH</i>	<i>GAGTCAACGGATTTGGTCGT</i>	<i>GACAAGCTTCCCCTTCTCAG</i>
<i>ID2</i>	<i>TTGTCAGCCTGCATCACCAGAG</i>	<i>AGCCACACAGTGCCTTGTCTGTC</i>
<i>K1</i>	<i>CAGCATCATTGCTGAGGTCAAGG</i>	<i>CATGCTGCCAGCAGTGATCTG</i>
<i>K3</i>	<i>ACGTGACTACCAGGAGCTGATG</i>	<i>ATGCTGACAGCACTCGGACACT</i>
<i>K5</i>	<i>GCTGCCACATGAACAAGGTGG</i>	<i>ATGGAGAGACCACCTGAGGTGT</i>
<i>K10</i>	<i>CCTGCTTCAGATCGACAATGCC</i>	<i>ATCTCCAGGTCAGCCTTGGTCA</i>
<i>K12</i>	<i>AGCAGAATCGGAAGGACGCTGA</i>	<i>ACCTCGCTTGTCTGACTGAA</i>
<i>K14</i>	<i>TGCCGAGGAATGGTTCTTACC</i>	<i>GCAGCTCAATCTCCAGGTTCTG</i>
<i>K15</i>	<i>AGGACTGACCTGGAGATGCAGA</i>	<i>TCCGCTCAATCTCCACATTGACC</i>
<i>K19</i>	<i>AGCTAGAGGTGAAGATCCGCGA</i>	<i>GCAGGACAATCCTGGAGTTCTC</i>
<i>MEIS1</i>	<i>AAGCAGTTGGCACAAGACACGG</i>	<i>CTGCTCGGTTGGACTGGTCTAT</i>
<i>MMP9</i>	<i>GCCACTACTGTGCCCTTGTAGTC</i>	<i>CCCTCAGAGAATCGCCAGTACT</i>
<i>MMP10</i>	<i>TCCAGGCTGTATGAAGGAGAGG</i>	<i>GGTAGGCATGAGCCAAACTGTG</i>
<i>NR2F2</i>	<i>TGCACGTTGACTCAGCCGAGTA</i>	<i>AAGCACACTGAGACTTTTCTCTGC</i>
<i>NOTCH1</i>	<i>GGTGAAGTCTCTGAGGAGATC</i>	<i>GGATTGCAGTCTGCCACGTTGA</i>
<i>NOTCH3</i>	<i>TACTGGTAGCCACTGTGAGCAG</i>	<i>CAGTTATCACCATTGTAGCCAGG</i>
<i>ODZ3</i>	<i>GGACAAGGCTATCACAGTGGAC</i>	<i>TTCTGAGGGAGCCGTCATAACC</i>
<i>PAX6</i>	<i>TGTCCAACGGATGTGTGAGT</i>	<i>TTTCCAAGCAAAGATGGAC</i>
<i>PDGFA</i>	<i>CAGCGACTCCTGGAGATAGACT</i>	<i>CGATGCTTCTTCTCCCGAATG</i>
<i>PPARG</i>	<i>AGCCTGCGAAAGCCCTTTGGTG</i>	<i>GGCTTCACATTCAGCAAACCTGG</i>
<i>PRDM8</i>	<i>CTGTGCTCTGAGCCATACTTCC</i>	<i>CCTTCTGAGGAACCAATTTGCTGC</i>
<i>TGFBI</i>	<i>AGGACTGACGGAGACCCCTCAAC</i>	<i>TCCGCTAACCAGGATTTTCATCAC</i>
<i>WNT7A</i>	<i>TGCCCGGACTCTCATGAAC</i>	<i>GTGTGGTCCAGCACGCTCTTG</i>
Gene (Rabbit)	Forward Primer	Reverse Primer
<i>GAPDH</i>	<i>GCGAGATCCC GCCAACATCAAGT</i>	<i>AGGATGCGTTGCTGACAATC</i>
<i>PAX6</i>	<i>GTATTCTTGCTTCAGGTAGAT</i>	<i>GAGGCTCAAATGCGACTTCAGCT</i>
Primers used for PAX6 transduction		
<i>PAX6 InF</i>	<i>TTCCCGAATTC TGACACCCATGCAGATGCAAAAGTCCAAGTCTGGACAATCAAACGTTGCCAACGGATGTG</i>	
<i>PAX6 InR</i>	<i>CACATCCGTTGGACACGTTTTGATTGTCCAGCACTTGGACTTTTGCATCTGCATGGGCTGCAGAATTCGGGAA</i>	

Extended Data Table 1b. Summary of rabbit transplantation results

GFP-labeled donor cells	Regeneration and re-epithelization	Rabbit number	
		Opaque and vascularized corneal surface	Died from systemic infection or unrelated complications
LSCs	3	0	0
PAX6+ SESC	5	0	2
shPAX6 LSCs	0	4	1

a. Primer sequences for human and rabbit genes used in this study. b. Corneal regeneration and re-epithelization were arrayed three months after transplantation.